Atmospheric characterization of cold exoplanets with a 1.5-m space coronagraph

Anne-Lise Maire[a], Raphaël Galicher[b], Anthony Boccaletti[a], Pierre Baudoz[a], Jean Schneider[c], Kerri Cahoy[d], Daphne Stam[e], and Wesley Traub[f]

[a]LESIA, Paris Observatory, CNRS, 5 pl. J. Janssen, 92195 Meudon, France;
[b]Herzberg Institute of Astrophysics, 5071 West Saanich Road, Victoria, BC V9E 2E7, Canada;
[c]LUTh, Paris Observatory, CNRS, 5 pl. J. Janssen, 92195 Meudon, France;
[d]NASA Ames Research Center, Moffett Field, CA 94035, USA;
[e]SRON, Sorbonnelaan 2, 3584 CA Utrecht, The Netherlands;
[f]JPL, California Institute of Technology, 4800 Oak Grove Drive, Pasadena, CA 91109, USA;

ABSTRACT

Several small space coronagraphs have been proposed to characterize cold exoplanets in reflected light. Studies have mainly focused on technical feasibility because of the huge star/planet flux ratio to achieve in the close-in stellar environment (10^8–10^{10} at $0.2''$). However, the main interest of such instruments, the analysis of planet properties, has remained highly unexplored so far. We performed numerical simulations to assess the ability of a small space coronagraph to retrieve spectra of mature Jupiters, Neptunes and super-Earths under realistic assumptions. We describe our assumptions: exoplanetary atmosphere models, instrument numerical simulation and observing conditions. Then, we define a criterion and use it to determine the required exposure times to measure several planet parameters from their spectra (separation, metallicity, cloud and surface coverages) for particular cases. Finally, we attempt to define a parameter space of the potential targets. In the case of a solar-type star, we show that a small coronagraph can characterize the spectral properties of a 2-AU Jupiter up to 10 pc and the cloud and surface coverage of super-Earths in the habitable zone for a few stars within 4–5 pc. Potentially, SPICES could perform analysis of a hypothetical Earth-size planet around α Cen A and B.

Keywords: numerical simulations, high angular resolution techniques, high-contrast imaging techniques, exoplanets, integral field spectrometry

1. INTRODUCTION

Direct imaging of extrasolar planets is one of the most challenging task in modern astrophysics. Since the end of the previous century, many concepts have been developed such as coronagraphy,[1–3] nulling interferometry,[4] external occulters[5] and Fresnel arrays.[6] In particular, conceptual studies were performed to consider the feasibility of large aperture coronagraphs and large baseline interferometers for the detection of Earth twins from space. These studies identified areas of technological development that need to be first addressed, which will postpone the realization of Terrestrial Planet Finder missions until ∼2025–2030. Meanwhile, observations have demonstrated the extreme diversity of planets. This led to a growing consensus within the community that we will need to study all planet types in order to have a complete understanding of their formation and evolution.[7] To address some parts of these questions, a family of small space missions (mainly coronagraphs) have been proposed for analyses of ice giants and super-Earths.[8,9] The study of these missions has mainly focused on technical feasibility, as it is a challenge to achieve large contrast close to a bright star.[10–12] Another area of study is the estimated number of observable exoplanets of a given type,[8,9] based on assumptions of their density distribution. The main interest of such missions, the atmospheric characterization, however, has remained highly unexplored so far. For instance, Cahoy et al.[13] analyze colors and coarse spectra (R = 5 and R = 15) of Jupiter and Neptune atmosphere models, but without including instrument limitations such as throughput and noise. We discuss in this paper the contrast and science performance of a small space coronagraphic telescope, in the

---

framework of the SPICES mission (see Ref. 14, and the companion paper published in these proceedings). We present the numerical model of the instrument and the assumptions used for our study in Sec. 2. In Sec. 3, we analyze the sensitivity of the instrument contrast to different sources of detection noise. Finally, we discuss the science cases our instrument can address for two planet types in Sec. 4. For further details, we refer the reader to Maire et al.[15]

2. MODELS AND HYPOTHESES

In this section, we describe the hypotheses on the numerical model of the instrument and on the planetary spectra we used for our performance analysis.

2.1 Instrument

The conceptual baseline of the SPICES instrument is shown in the left panel of Fig. 1. It consists of:

- a high-quality off-axis primary mirror;

- a polarization modulator to select the polarized flux component to measure;

- a 64×64 deformable mirror (DM) to correct for the wavefront aberrations induced by imperfect optics;

- a optical vortex coronagraph[3] providing a small inner working angle (IWA, $\sim 2\ \lambda/D$) and a high throughput (>90%);

- a micro-lenses based integral field spectro-polarimeter[16] which samples the field of view and disperses the fluxes on a large detector (4000×4000 pixels). An algorithm reconstructs a (x, y, λ) data cube from the spectra;

- a wavefront sensor which measures the wavefront aberrations from the science images and drives the DM. The wavefront sensing from the science images avoids the performance degradation of the correction due to differential errors between the science and the wavefront sensing channels. We use the self coherent camera, a very simple modification of the Lyot stop of the coronagraph which also provides a further means to remove the stellar residuals non corrected by the DM.[17, 18]

We built a numerical model of the instrument in the Interactive Data Language*. It works in three steps:

1. It generates non coronagraphic and coronagraphic image cubes of an on-axis source (the star) and off-axis source(s) (the planet(s)). We assume that the data cubes are extracted from the spectra without errors, but account for the flat field variations of detector pixels.

2. It normalizes the fluxes with blackbody spectra for the star and realistic spectra for the planet(s)[13, 19] and simulates detection noise from different sources (stellar photons, zodiacal light, exo-zodiacal cloud, detector read-out and flat field variations).

3. It performs the calibration processing of the speckles by the self coherent camera and measures the spectra of the planet(s).

The simulation parameters were optimized to satisfy the science requirements of SPICES, i.e. a contrast of 10^{-9} at 2 λ/D and 10^{-10} at 4 λ/D.[14] Pointing errors of the star onto the coronagraph are one of the main critical aspects of the mission, so a specific procedure was designed to control these errors at a level of 0.2 mas.[14] We assessed from simulations that this value does not degrade the instrument contrast above the requirements (study not shown) and do not account for pointing errors in the simulations presented in this paper. Contrary to SPICES' design,[14] the whole bandwidth (0.45–0.9 μm) is simulated in a sole optical train. We assume an achromatic optical vortex coronagraph for all the spectral band. Each image of a spectral channel is simulated by co-adding 15 monochromatic images taken uniformly in the channel band. We propagate the light from the
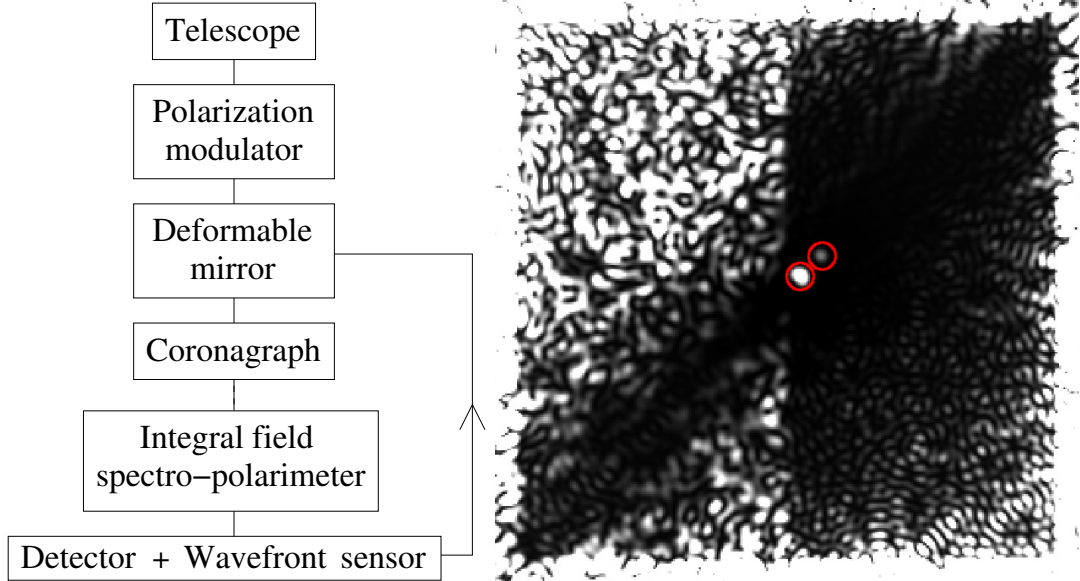
---

*www.exelisvis.com

Figure 1. Left: SPICES conceptual baseline. Right: Central part of a simulated image obtained with the SPICES instrument without detection noise except the speckle noise. The size of the field of view is 64×64 $(\lambda/D)^2$ (6×6 arcsec^2) while the DM correction area is 32×64 $(\lambda/D)^2$ (right half of the field of view). We added two planets of contrast 10^{-8} and 10^{-9} at 2.2 λ/D and 5.4 λ/D respectively (red circles).

telescope pupil to the detector matrix using Fourier transforms.[20] By doing this, we consider that all aberrations (phase and amplitude) are located in planes conjugated to the telescope pupil, so the speckle pattern does not undergo a partial decorrelation with the wavelength.[21] Such an effect will not impact the wavefront estimation with the self coherent camera since the latter processes each spectral channel separately. However, it will limit the performance of the DM correction because SPICES' concept uses a single DM to correct for the wavefront aberrations on all the bandwidth.[22] We assume that the aberrations are due to optical imperfections of the primary mirror. The phase aberrations are induced by optical path differences of 20 nm rms which are modeled with a power spectral density in f^{-3}, where f is the spatial frequency of the optical defect.[23] The amplitude aberrations are set to 0.1% and are simulated with a power spectral density in f^{-1}. The impact of amplitude aberrations is the reduction of the DM correction area by a factor 2 in size (Fig. 1, right panel). We assume that the self coherent camera perfectly estimates for the wavefront aberrations and project the estimated wavefront on the DM using the algorithm of Ref. 23.

The hypotheses of the sources of detection noise are the following. The global instrument throughput (optical transmission × detector quantum efficiency) is set to 16%. We consider the zodiacal light to be a uniform background of magnitude V = 23.1 mag.arcsec^{-2}.[24] We use the Zodipic algorithm[25] to simulate an exo-zodiacal cloud around the star. The impact of the exozodi intensity is analyzed in Sec. 3.2. We model the detector read-out noise as a gaussian noise. Its value is discussed in Sec. 3.2. The read-out noise in the image obtained for a total integration time is calculated by multiplying the read-out noise level by the number of single exposures used. We assume single exposures of 1000 s[26] and a detector full well capacity of 300 000 ke-. Finally, we model the flat field variations of the detector as a gaussian noise of mean 1 and rms of 0.5%.

2.2 Planetary spectra

The planetary spectra we used assume ~4.5-Gyr planets in radiative equilibrium with the flux of a Sun-like parent star. Moreover, they are derived for discrete values of separations (0.8, 2, 5 and 10 AU for the models of Ref. 13 and 1 AU for those of Ref. 19). We cannot extrapolate the planet spectra to any separations around any stars, because the reflected flux depends strongly on these parameters.[13] Instead, we calculate the corresponding separation for a given stellar luminosity, considering that the flux is conserved and the equilibrium atmospheric

temperature T_{eq} and the Bond albedo A_B only depend on the incident stellar flux at the planet position $L_\star/a^2$. The standard formula of flux conservation is:

$$4\pi R_p^2 \, \sigma \, T_{eq}^4 \; = \; (1 - A_B) \, \pi \, R_p^2 \, \frac{L_\star}{4 \, \pi \, a^2} \tag{1}$$

where R_p is the planet radius and σ is Stefan's constant Applying our hypotheses, this equation becomes:

$$L_\star \propto a^2 \quad \Rightarrow \quad a_{S_p} \; = \; a_{G2} \, \sqrt{L_{S_p}} \tag{2}$$

where a_{S_p} is the star-planet separation for a star of spectral type S_p, a_{G2} the star-planet separation for a G2 star and L_{S_p} the star luminosity in solar units. For instance, the separation sequence 0.8, 2, 5 and 10 AU considered by Cahoy et al.[13] for a solar-type star becomes 0.24, 0.6, 1.5 and 3 AU for a M0-type star (see the right panel of Fig. 4), assuming a luminosity of 0.09 solar units.

Finally, we obtain the contrast of a planet around a host star of type S_p:

$$C(\lambda) = A(\lambda, \alpha) \, \frac{R_p^2}{a_{S_p}^2} = A(\lambda, \alpha) \, \frac{R_p^2}{a_{G2}^2 \, L_{S_p}} \tag{3}$$

We use Eqs. (2) and (3) to derive the star-planet separations and contrasts in Sec. 3.

3. CONTRAST PERFORMANCE

Here we analyze the sensitivity of the instrument contrast to several sources of detection noise: speckle noise, detector read-out noise, intensity of the exo-zodiacal cloud and stellar photon noise.

3.1 Instrument contrast

To have a clear and simple view of SPICES' performance, we plot radial profiles averaged on all the spectral channels instead of radial profiles for all channels. Fig. 2 shows the instrument contrast for a solar-type star against the physical separation in AU and three star distances. The performance is limited at short separations by the coronagraph IWA ($\sim 2 \, \lambda/D$, Sec. 2), and at large separations by the size of the DM corrected area (cut-off at 32 λ/D). As we express the x-axis in AU, the contrast curve scales with the star distance. We also plot the positions of Jupiter-like planets, Neptune analogs, and 2.5 Earth radii (R_E) cloudy super-Earths. Since Stam[19] modeled only one separation (1 AU), we assume that the super-Earth properties do not evolve with separation for the considered range (1–3 AU). For stars at 20 pc, the farthest Jupiters (5 and 10 AU) and Neptunes (5 AU) are detected with SNR > 5. The 10-AU Neptune is below the curve (SNR $\simeq 4.5$). For a 10-pc star, the same planets are still detected as well as planets as close as 2 AU. For the closest star we consider (3 pc), planets as close as 1 AU are very well detected ($100 \lesssim$ SNR $\lesssim 1000$). In this case, the 10-AU Jupiter and 5-AU Neptune are not detected with SPICES because of the speckle calibration degradation with angular separation. Solutions may exist to improve the detection at these large angular separations ($\gtrsim 18 \, \lambda/D$) such as spectral deconvolution.[27]

In addition, we plot the averaged contrast levels for zodiacal light and a 1-zodi exodisk, both for a star distance of 10 pc (they increase as the square of the star distance). Although the instrument concept can reduce speckle noise below a contrast of 10^{-10}, the final performance is limited by these extended background sources. The considered exo-zodiacal disk limitation is at the level of Neptunes and super-Earths. Therefore, to obtain a correct estimation of planet fluxes, the zodiacal and exo-zodiacal contributions must be carefully calibrated and removed. In particular, the exo-zodiacal disk intensity has been identified as critical for Earth-twin detection with space nulling interferometers.[28] However, the intensity of nearby exo-zodiacal clouds is still largely unknown so exo-disk surveys have been recommended to prepare target lists of faint exo-disks.[29–31] In the case of SPICES, the problematic is different as we do single-aperture imaging. The exact procedure to account for zodiacal and exo-zodiacal contributions remains to be defined but it is a data reduction issue. In the following, we consider the model distribution of both zodiacal and exo-zodiacal intensities can be subtracted from the data but the photon noise of these sources is accounted for. The latter may still limit the contrast performance (Sec. 3.2).
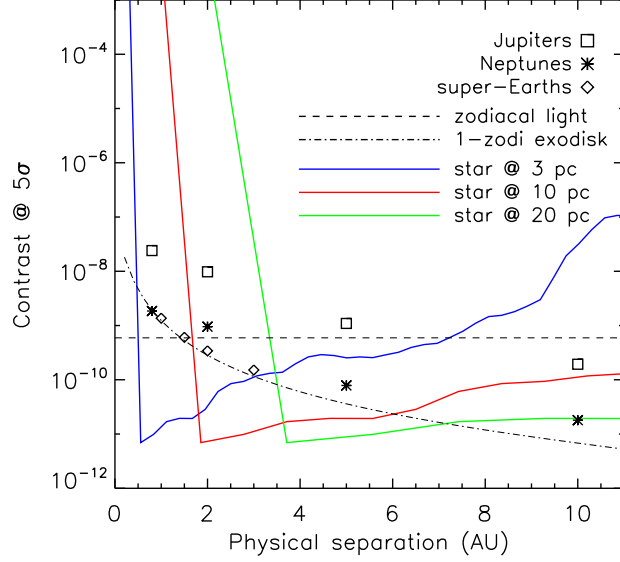
Figure 2. Mean radial profiles of the 5-σ detection level of SPICES' contrast (solid curves) compared to averaged planet contrasts calculated for a solar-type star (symbols). For comparison, we also plot the mean contrast of the zodiacal light (horizontal dashed line) and a 1-zodi exodisk (dot-dashed curve), both for a star at 10 pc.
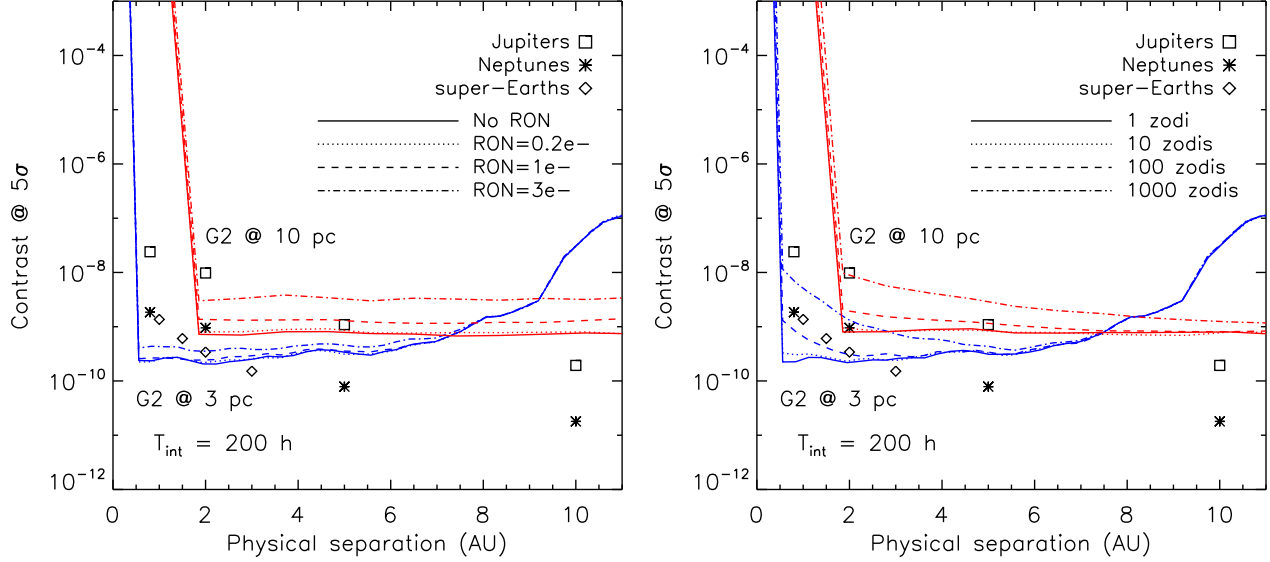

Figure 3. Mean radial profiles of the 5-σ detection level for different levels (indicated by the line style) of read-out noise of the detector (left) and of exozodi intensity (right). The curves are calculated for two star distances, 3 pc (blue curves) and 10 pc (red curves) accounting for photon noise.

3.2 Sensitivity to detection noise

We now discuss the sensitivity of the instrument contrast on different sources of detection noise. For this study, we assume a total integration of 200 h per target, which is a good trade-off between achieving high contrasts and observing a large number of targets during the mission. We show the impact of photon and read-out noise on SPICES' performance for the case of a G2 star at 3 and 10 pc in the left panel of Fig. 3. We note that read-out noise is a major limitation for the farthest star but not for the closest. Indeed, the full well capacity of the detector (300 000 ke-) is not filled after a 1 000-s exposure in both cases. The number of single exposures
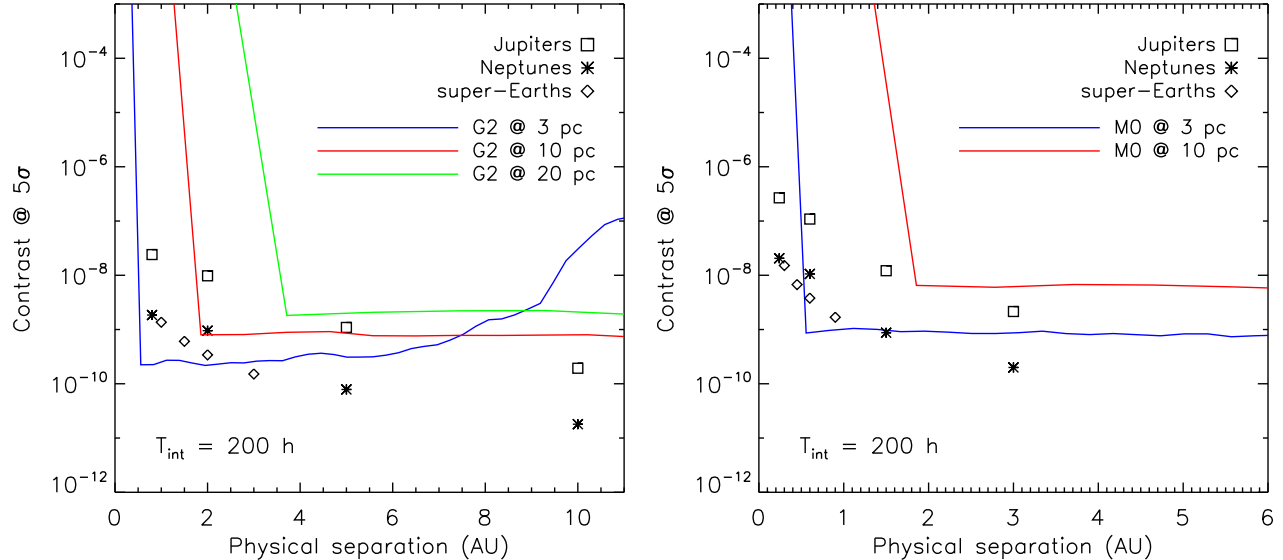
Figure 4. Mean radial profiles of the 5-σ detection level for a G2-type star (left) and a M-type star (right). The curves are plotted for several star distances assuming photon noise and a total integration of 200 h. The planet/star contrast and star-planet separation are derived from Eqs. 2 and 3.

and read-out noise level are thus the same, but the photon count is greater for the closest star. We note that the dozen of stars located within 3 pc have types later than G so read-out noise will not be a fundamental limitation for these stars. We base the read-out noise requirement on the farthest star and set its value to 0.2 e- rms per pixel. Electron multiplying CCDs can achieve such a low read-out noise, and a large set of devices have been qualified for space during the preparation of the *Gaia* mission.[32]

As indicated in the previous section, an exo-disk can prevent the detection of faint planets if its photon noise becomes too important. The right panel of Fig. 3 analyzes the exozodi level that may hamper the detection of SPICES' targets, for two distances of a solar-type star. We find that the exo-disk photon noise does not significantly limit the performance up to 10 zodis, but begins preventing the Neptune and super-Earth detection when larger than 100 zodis. For exposures shorter than 200 h (more dominant photon noise), the acceptable exozodi level is lower. In the remainder of this paper, we consider a exo-zodiacal cloud of 1 zodi.

The last study of this section tests the detectability of planets for several stellar types. Figure 4 presents the 5-σ detection levels for two stars of type G2 and M0 and several distances (3, 10, and 20 pc). We consider the star-planet separations of Sec. 2.2 and we apply Eq. (3) to find the wavelength-averaged planet contrasts. For a G2 star (Fig. 4, left), SPICES can potentially access jovian planets, icy giants and super-Earths with separations smaller than ~6, ~3 and ~2 AU respectively. No planet is detected at distances larger than ~10 pc. The detectability of the closest planets (0.8 to 2 AU) will be limited by the coronagraph IWA (~2 λ/D) for stars at 4 to 10 pc. The very close M stars (Fig. 4, right) at 3–5 pc are of great interest for detecting Jupiter-like planets in the 0.5–4 AU range as well as super-Earths in close orbits at 0.5–1 AU.

4. SCIENCE PERFORMANCE

We discuss in this section SPICES' performance for characterization of planets orbiting a solar-type star. We first define a criterion for disentangling planetary spectra with different properties based on theoretical models. Then, we study the science cases for typical targets. Finally, we determine a preliminary sample of potential targets.

4.1 Criterion of characterization

The question is to know if a measured spectrum S is reproduced by one of two model spectra noted M_i (i refering to the model index, $i = 1,2$). This depends on the noise of the measured spectrum $N = S/\mathrm{SNR}$. We define the

Table 1. Values of SNR$_r$ derived from Eq. (5).

Planet	Parameter	SNR$_r$	Note
Jupiter	0.8/2 AU	15	
Jupiter 0.8 AU	metallicity 1/3x	30	
Jupiter 2 AU	metallicity 1/3x	30	CH$_4$ bands
Jupiter 5 AU	metallicity 1/3x	30	CH$_4$ bands
Neptune	0.8/2 AU	15	
Neptune 0.8 AU	metallicity 10/30x	30	
Neptune 2 AU	metallicity 10/30x	25	CH$_4$ bands
Forest Earth	0/50/100% clouds	25	blue channels
Ocean Earth	0/50/100% clouds	25	blue channels
Clear Earth	0/50/100% forests	12	red channels
50% cloudy Earth	0/50/100% forests	30	red channels
Cloudy Earth	0/50/100% forests	220	red channels

following criteria of comparison of S to M_i:

$$crit_i = \mathrm{median}_\lambda \left(\frac{S(\lambda) - M_i(\lambda)}{S(\lambda)} \times \right) \mathrm{SNR} \tag{4}$$

where the median is calculated over the spectral channels and SNR is assumed nearly constant on the measured spectrum. We choose the median because it accounts well for the overall quality of a spectrum. For a given measurement (S, N), the model which best matches the measured spectrum gives the lowest criterion value. In this paper, we use theoretical models to assess the instrument performance and to set the SNR required to measure differences between them ($S = M_1$ and $M_i = M_2$). We consider that the models are differentiated when their difference is 10 times above the measured noise so $crit_i = 10$. Inverting Eq. (4) and calling SNR$_r$ the value of the required SNR, we finally obtain:

$$\mathrm{SNR}_r = 10 \times \frac{1}{\mathrm{median}_\lambda \left(\frac{M_1(\lambda) - M_2(\lambda)}{M_1(\lambda)} \right)} \tag{5}$$

As an example, when we study the metallicity (Sect. 4.2), M_1 will be the lowest metallicity model and M_2 the highest metallicity model. We consider different spectral bandwidths to determine SNR$_r$ (Eq. (5)) when analyzing different planetary properties. For instance, metallicity strenghtens the bands (Fig. 6), and surface coverage alter the spectrum at red wavelengths (Fig. 7).

We give the calculated SNR$_r$ in Table 1 and we specify the spectral channels in the last column. We stress the point that the SNR$_r$ values correspond to the spectrum of the brightest planet considered for each analyzed property: for instance, the low-metallicity planets for the Jupiters and Neptunes (Sec. 4.2) and the forest planets for the analysis of the super-Earth surfaces (Sec. 4.3). The SNR$_r$ values are used to derive the exposure times required to disentangle the planet spectra in the next two sections. We perform these simulations for five independent realizations of speckle pattern. We then average our results to minimize the impact of an optimistic or pessimistic speckle pattern. To save computing time, we use the same five speckle patterns for all planet cases, but we randomly change the photon and read-out noise. We assume the planet position to be perfectly known and integrate the planet flux within apertures of diameter 1 λ/D for each spectral channel. The 1-σ error bars shown in the plots account for the variation of both speckle and noise realizations.

4.2 Science cases for giant planets

In addition to the identification of spectral features (continuum, molecular absorption bands), the two science cases we address for giant planets are the measurement of the Rayleigh scattering and the metallicity enhancement of the atmosphere. Rayleigh scattering occurs for close-in planets ($\sim$1 AU) because the atmospheric temperature
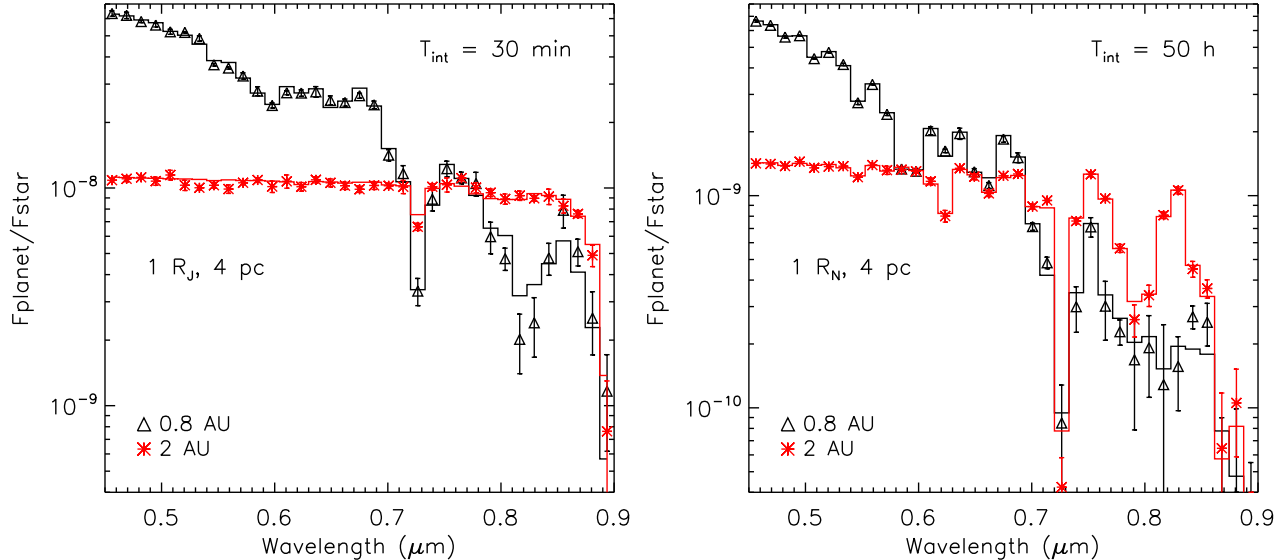
Figure 5. Simulated (symbols) and theoretical spectra of Jupiter (left) and Neptune (right) analogs for two separations to a solar-type star. For 0.8-AU planets, the atmospheric temperature is warm enough to prevent the cloud condensation and the dominant diffusion source is the Rayleigh scattering by the gas molecules. For 2-AU planets, water clouds form and flatten out the spectrum continuum.

is high enough to prevent the cloud formation.[13] This can be used to constrain the physical separation of planets. Considering the theoretical models (solid lines in Fig. 5), giant planet spectra mostly differ in the blue, where Rayleigh scattering dominates for a planet at 0.8 AU. The application of the criterion defined in Eq. (5) indicates that $SNR_r \simeq 15$ permits to distinguish between the atmospheres of two giants at 0.8 and 2 AU respectively (Table 1). This performance is achieved in ~30 min and 50 h for respectively Jupiters and Neptunes at a distance of 4 pc. This distance corresponds to the upper limit at which a separation of 0.8 AU is accessible to SPICES. We plot the spectra as they would be measured by the instrument with 1-σ error bars in Fig. 5. As expected, for both cases, the blue half of the bandwidth is the region where the spectra can be distinguished with no ambiguity. SPICES will thus be able to measure Rayleigh scattering and constrain the separation for planets around a few nearby Sun analogs, because of its small angular resolution.

The planet atmospheric metallicity is a tracer of its formation process.[13] As indicated in Table 1, this requires $SNR_r \simeq 30$ for giant planets at 2 AU with metallicity factors of 3. For the Jupiters, this value is achieved within the distance for which our instrument can resolve such a planet ($\leq$10 pc). In particular, an integration time of 30 h satisfies the criterion for a solar-type star at 10 pc (Fig. 6, left panel). For the Neptunes, their fainter contrast limits the instrument sensitivity to planets within 5–6 pc (Fig. 6, right panel). The spectral differences are larger in the methane bands: 0.73 and 0.89 μm for the Jupiters, and 0.62, 0.66 and 0.79 μm for the Neptunes.

4.3 Science cases for rocky planets

Information about the planet surface can be obtained for moderate cloud coverage, because it produces noticeable signatures (Fig. 7). The differences between surface types are larger for a clear atmosphere, especially in the half red part of the spectral range. We consider three generic cases of planets with an ocean, an equally mixed surface of ocean and forest, and a forest. To separate these cases, $SNR_r \sim 12$ (Table 1) is required on the forest model and $SNR_m > 12$ is achieved in a ~200-h observation for the distance limit imposed by the coronagraph IWA (5 pc, left panel of Fig. 7). SPICES can distinguish these three cases for 2.5-R_E terrestrial planets on a 1-AU orbit around a Sun analog within 5 pc. If we consider 50% cloud coverage, surface effects are more difficult to distinguish and would require $SNR_r \sim 30$ in the red part (Table 1). The SNR_r criterion is not satisfied within an exposure time of 200 h for a target at 5 pc, in turns the limit is rather 4 pc (Fig. 7, right panel).
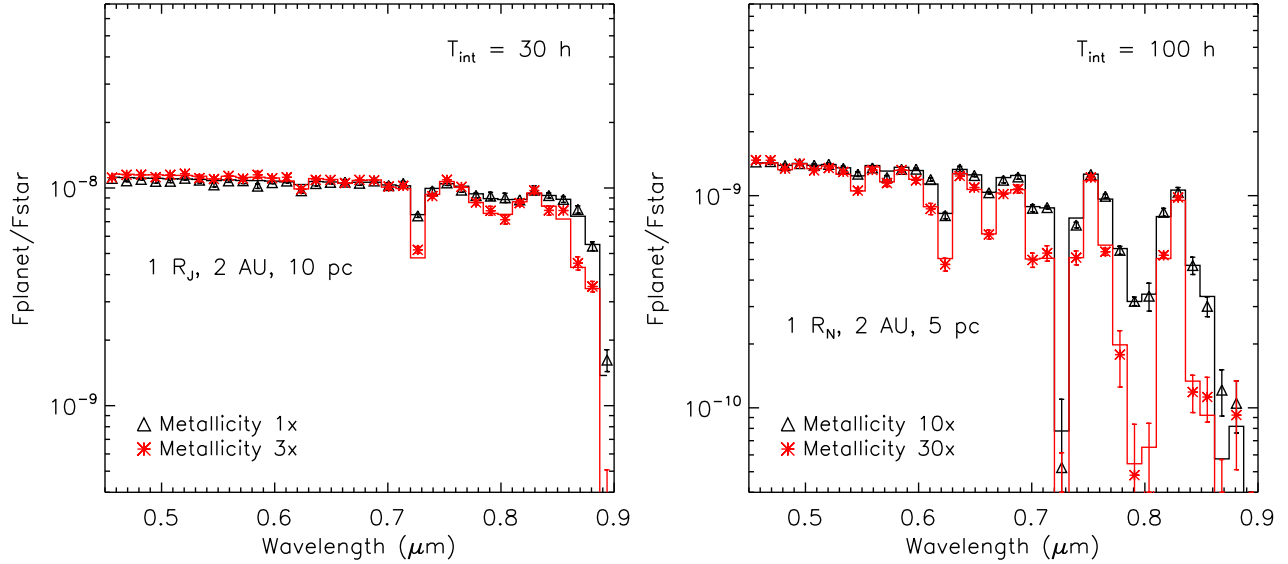
Figure 6. Simulated (symbols) and theoretical spectra of Jupiter (left) and Neptune (right) analogs for two atmospheric metallicity enhancements. Higher metallicity enhancement strenghtens the methane absorption bands: 0.73 and 0.89 μm for the Jupiters, and 0.62, 0.66 and 0.79 μm for the Neptunes.
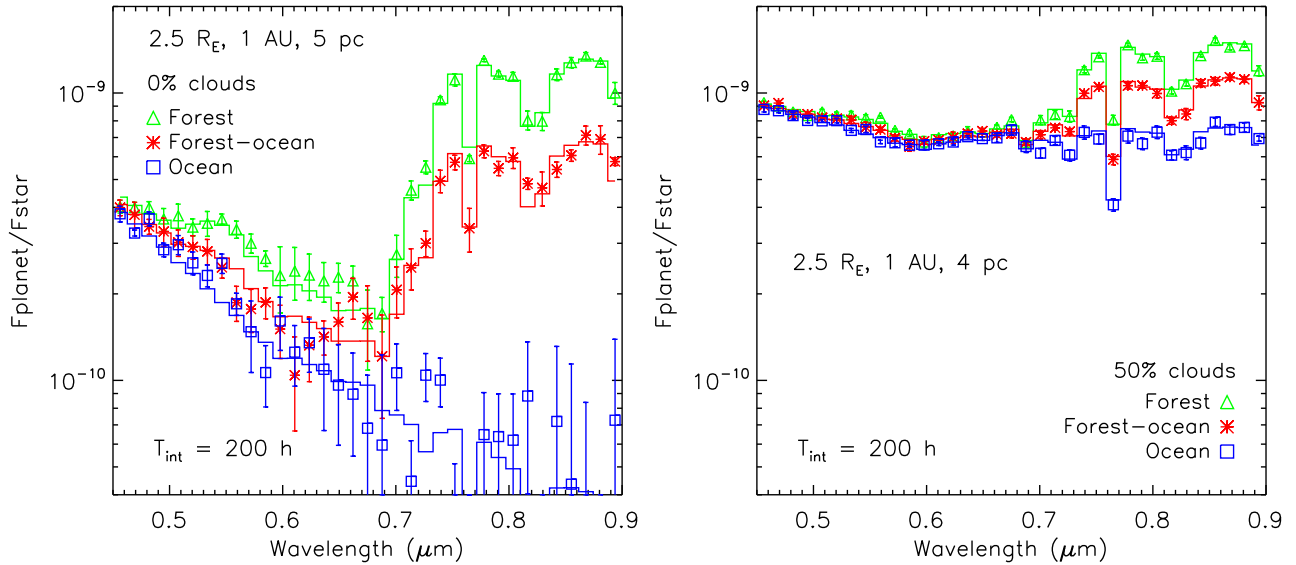

Figure 7. Simulated (symbols) and theoretical spectra of 2.5-R_E super-Earths with cloud-free (left) and 50% cloudy (right) atmospheres for different surface coverage (forest, equal forest-ocean mix and ocean). The surface type alter the spectra especially in the half red part of the bandwidth.

Molecular oxygen and water absorptions as well as the "red edge" can still be measured ($SNR_m > 11$, 21 and 26 respectively).

4.4 Potential targets

In this section, we study the volume of the planet sample around solar-type stars which can be characterized (metallicity, cloud coverage, surface type) with SPICES, assuming a maximum exposure time of 200 h (Sec. 3.2). The models used and the corresponding SNR_r are listed in Table 1. We consider that the planet flux increases as the square of its radius and that the atmosphere composition and structure remain the same. We consider
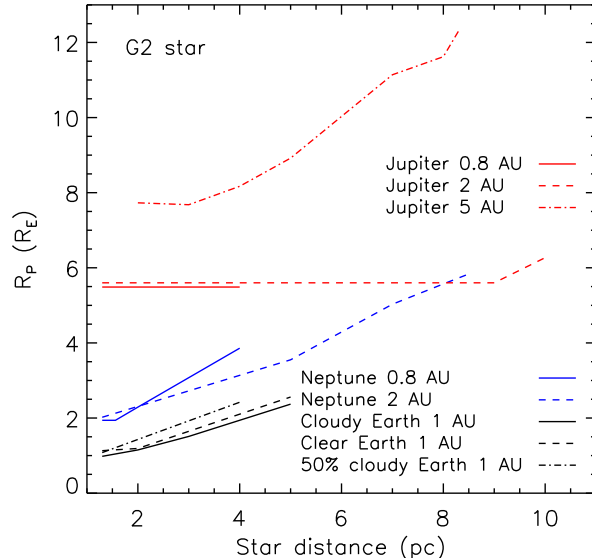
Figure 8. Minimum radius of model planets around a solar-type star for which the SNR requirement for characterization is meet (Table 1). We slightly offset for clarity the curves of the 0.8-AU Jupiter.

the following radius ranges for the planets: $R_p \leq 2.5\ R_E$ for the Earths, $0.5\ R_N \leq R_p \leq 1.5\ R_N$ for the Neptunes and $0.5\ R_J \leq R_p \leq 1.1\ R_J$ for the Jupiters.[33, 34] R_J and R_N refer to Jupiter and Neptune radii respectively.

Figure 8 shows the results of this analysis (with radii in R_E units). The colors indicate the planet type (Jupiter, Neptune or Earth) and the line styles the planet model. For the 0.8- and 2-AU Jupiters, SPICES reaches the lowest radius we consider ($0.5\ R_J \sim 5.5\ R_E$) for all stars within 4 and 10 pc respectively (distances limited by the instrument resolution, Sec. 2.1). About 20 G stars could be probed for Jupiters at 2 AU, while a few stars could be searched for Jupiters at 0.8 AU. For a Jupiter at 5 AU, the upper limit in radius is reached when the star is at 8.5 pc ($1.1\ R_J \sim 12\ R_E$). The radius linearly decreases as the star distance decreases down to 8 R_E at 4 pc (flux proportional to the square ratio of the planet radius to the star distance). At shorter distances, the deviations from the linearity are due to the increase of the speckle noise level. Indeed, when the star distance decreases, the angular separation of the star-planet system increases and the speckle background increases, especially towards the edges of the dark hole (Fig. 2, right panel). As for Neptune-like planets, the minimum radius scales nearly linearly with distance from $\sim$ 2 to 4 R_E at 0.8 AU, and from 2 to 6 R_E at 2 AU. SPICES can characterize cloudy and clear telluric planets at 1 AU around a few G2 stars up to 5 pc (IWA limitation). Potentially, it is able to reach Earth-size planets around α Cen A ($\sim$ 1.3 pc). We also studied the case of A0 and M0 stars (the detailed study can be found in Maire et al.[15]). In the former case, the instrument could study the metallicity of cloud-free Jupiters closer than 17 pc, while in the latter case, cloudy Jupiters and Neptunes would be accessible at distances $\geq$7.5 pc and $\geq$3 pc respectively, and super-Earths at distances $\geq$3 pc.

5. CONCLUSION

In this paper, we presented an analysis and an estimation of the performance of a small coronagraphic space mission operating in the visible, in the framework of the SPICES mission.[14] From numerical simulations of the instrument concept, we first determined that the contrast reached by the instrument meets the top-level requirements ($\sim 10^{-9}$ at 2 λ/D and $\sim 10^{-10}$ at 4 λ/D). Then, we analyzed the impact of different sources of noise: detector read-out noise, exo-zodiacal intensity and stellar photon noise. We confirmed previous analyses that the exodisk intensity might be a major limitation for the characterization of faint planets, like Neptunes and super-Earths, because it biases the planet photometry (for values $\gtrsim$1 zodi) and adds photon noise ($\gtrsim$a few 10 zodis). Exodisk intensity calibration and target selection will be necessary to reduce this limitation, but local structures (gaps, clumps, etc) will still remain. SPICES could detect a large variety of planets within $\sim$12 pc

for a G2 star and ∼7.5 pc for a M0 star. We also discussed the instrument abilities for disentangling planetary properties from realistic spectra for typical targets around solar-type stars. The results are very encouraging since it could characterize the atmosphere (molecular species, metallicity for instance) of Jupiters and Neptunes up to 10 pc and 6 pc respectively. The cloud and surface coverage of a super-Earth would also be characterized for systems closer than 5 pc. We also estimated the minimum radius for the planets SPICES could detect. Extending our results to all stellar types, we estimate a potential target list of ∼300 stars.

REFERENCES

[1] Rouan, D., Riaud, P., Boccaletti, A., Clénet, Y., and Labeyrie, A., "The four-quadrant phase-mask coronagraph. i. principle," *PASP* **112**, 1479–1486 (2000).

[2] Guyon, O., "Phase-induced amplitude apodization of telescope pupils for extrasolar terrestrial planet imaging," *A&A* **404**, 379–387 (2003).

[3] Mawet, D., Riaud, P., Absil, O., and Surdej, J., "Annular groove phase mask coronagraph," *ApJ* **633**, 1191–1200 (2005).

[4] Bracewell, R. N., "Detecting nonsolar planets by spinning infrared interferometer," *Nature* **274**, 780 (1978).

[5] Cash, W., "Detection of Earth-like planets around nearby stars using a petal-shaped occulter," *Nature* **442**, 51–53 (2006).

[6] Koechlin, L., D., S., and P., D., "High resolution imaging with fresnel interferometric arrays: suitability for exoplanet detection," *A&A* **443**, 709–720 (2005).

[7] Schneider, J., Boccaletti, A., Aylward, A., Baudoz, P., Beuzit, J., Brown, R., Cho, J., Dohlen, K., Ferrari, M., Galicher, R., Grasset, O., Grenfell, L., Griessmeier, J., Guyon, O., Hough, J., Kasper, M., Keller, C., Longmore, A., Lopez, B., Martin, E., Mawet, D., Menard, F., Merin, B., Palle, E., Perrin, G., Pinfield, D., Sein, E., Shore, P., Sotin, C., Sozzetti, A., Stam, D., Surdej, J., Tamburini, F., Tinetti, G., Udry, S., Verinaud, C., and Walker, D., "Diversity among other worlds: Characterization of exoplanets by direct detection," *ArXiv e-prints* (2008). [arXiv:0811.2496].

[8] Guyon, O., Shaklan, S., Levine, M., Cahoy, K., Tenerelli, D., Belikov, R., and Kern, B., "The pupil mapping exoplanet coronagraphic observer (peco)," in [*SPIE Conf. Series*], *SPIE Conf. Series* **7731**, 773129 (2010).

[9] Trauger, J., Stapelfeldt, K., Traub, W., Krist, J., Moody, D., Mawet, D., Serabyn, E., Henry, C., Brugarolas, P., Alexander, J., Gappinger, R., Dawson, O., Mireles, V., Park, P., Pueyo, L., Shaklan, S., Guyon, O., Kasdin, J., Vanderbei, R., Spergel, D., Belikov, R., Marcy, G., Brown, R. A., Schneider, J., Woodgate, B., Egerman, R., Matthews, G., Elias, J., Conturie, Y., Vallone, P., Voyer, P., Polidan, R., Lillie, C., Spittler, C., Lee, D., Hejal, R., Bronowicki, A., Saldivar, N., Ealey, M., and Price, T., "Access: a concept study for the direct imaging and spectroscopy of exoplanetary systems," in [*SPIE Conf. Series*], *SPIE Conf. Series* **7731**, 773128 (2010).

[10] Trauger, J. T. and Traub, W. A., "A laboratory demonstration of the capability to image an earth-like extrasolar planet," *Nature* **446**, 771–773 (2007).

[11] Guyon, O., Pluzhnik, E., Martinache, F., Totems, J., Tanaka, S., Matsuo, T., Blain, C., and Belikov, R., "High-contrast imaging and wavefront control with a piaa coronagraph: Laboratory system validation," *PASP* **122**, 71–84 (2010).

[12] Belikov, R., Pluzhnik, E., Connelley, M. S., Witteborn, F. C., Greene, T. P., Lynch, D. H., Zell, P. T., and Guyon, O., "Laboratory demonstration of high-contrast imaging at 2 λ/d on a temperature-stabilized testbed in air," in [*SPIE Conf. Series*], *SPIE Conf. Series* **7731**, 77312D (2010).

[13] Cahoy, K. L., Marley, M. S., and Fortney, J. J., "Exoplanet albedo spectra and colors as a function of planet phase, separation, and metallicity," *ApJ* **724**, 189–214 (2010).

[14] Boccaletti, A., Schneider, J., Traub, W., Lagage, P.-O., Stam, D., Gratton, R., Trauger, J., Cahoy, K., Snik, F., Baudoz, P., Galicher, R., Reess, J.-M., Mawet, D., Augereau, J.-C., Patience, J., Kuchner, M., Wyatt, M., Pantin, E., Maire, A.-L., Vérinaud, C., Ronayette, S., Dubreuil, D., Min, M., Rodenhuis, M., Mesa, D., Belikov, R., Guyon, O., Tamura, M., Murakami, N., and Beerer, I. M., "Spices: Spectro-polarimetric imaging and characterization of exoplanetary systems," *Exp. Astron.* (2012). [arXiv:1203.0507].

[15] Maire, A.-L., Galicher, R., Boccaletti, A., Baudoz, P., Schneider, J., Cahoy, K., Stam, D., and Traub, W., "Atmospheric characterization of cold exoplanets using a 1.5-m coronagraphic space telescope," *A&A* **541**, A83 (2012).

[16] Antichi, J., Dohlen, K., Gratton, R. G., Mesa, D., Claudi, R. U., Giro, E., Boccaletti, A., Mouillet, D., Puget, P., and Beuzit, J.-L., "Bigre: A low cross-talk integral field unit tailored for extrasolar planets imaging spectroscopy," *ApJ* **695**, 1042–1057 (2009).

[17] Galicher, R., Baudoz, P., Rousset, G., Totems, J., and Mas, M., "Self-coherent camera as a focal plane wavefront sensor: simulations," *A&A* **509**, A31+ (2010).

[18] Baudoz, P., Boccaletti, A., Baudrand, J., and Rouan, D., "The self-coherent camera: a new tool for planet detection," in [*Direct Imaging of Exoplanets: Science & Techniques*], Aime, C. and Vakili, F., eds., *IAU Colloq.* **200**, 553 (2006).

[19] Stam, D., "Spectropolarimetric signatures of earth-like extrasolar planets," *A&A* **482**, 989–1007 (2008).

[20] Soummer, R., Pueyo, L., Sivaramakrishnan, A., and Vanderbei, R. J., "Fast computation of lyot-style coronagraph propagation," *Optics Express* **15**, 15935 (2007).

[21] Marois, C., Phillion, D. W., and Macintosh, B., "Exoplanet detection with simultaneous spectral differential imaging: effects of out-of-pupil-plane optical aberrations," in [*SPIE Conf. Series*], *Proc. of SPIE* **6269**, 62693M (2006).

[22] Shaklan, S. B. and Green, J. J., "Reflectivity and optical surface height requirements in a broadband coronagraph. 1.contrast floor due to controllable spatial frequencies," *ApOpt* **45**, 5143–5153 (2006).

[23] Bordé, P. J. and Traub, W. A., "High-contrast imaging from space: Speckle nulling in a low-aberration regime," *ApJ* **638**, 488–498 (2006).

[24] Giavalisco, M., Sahu, K., and Bohlin, R. C., "New estimates of the sky background for the hst exposure time calculator," STScI Instrument Science Report WFC3-ISR 2002 - 02 (2002).

[25] Kuchner, M. J., "A minimum-mass extrasolar nebula," *ApJ* **612**, 1147–1151 (2004).

[26] Robberto, M., "Nircam optimal readout modes," Tech. Rep. JWST-STScI-001721 (2009).

[27] Sparks, W. B. and Ford, H. C., "Imaging spectroscopy for extrasolar planet detection," *ApJ* **578**, 543–564 (2002).

[28] Cockell, C. S., Herbst, T., Léger, A., Absil, O., Beichman, C., Benz, W., Brack, A., Chazelas, B., Chelli, A., Cottin, H., Coudé du Foresto, V., Danchi, W., Defrère, D., den Herder, J.-W., Eiroa, C., Fridlund, M., Henning, T., Johnston, K., Kaltenegger, L., Labadie, L., Lammer, H., Launhardt, R., Lawson, P., Lay, O. P., Liseau, R., Martin, S. R., Mawet, D., Mourard, D., Moutou, C., Mugnier, L., Paresce, F., Quirrenbach, A., Rabbia, Y., Rottgering, H. J. A., Rouan, D., Santos, N., Selsis, F., Serabyn, E., Westall, F., White, G., Ollivier, M., and Bordé, P., "Darwin – an experimental astronomy mission to search for extrasolar planets," *Exp. Astron.* **23**, 435–461 (2009).

[29] Lunine, J. I., Fischer, D., Hammel, H., Henning, T., Hillenbrand, L., Kasting, J., Laughlin, G., Macintosh, B., Marley, M., Melnick, G., Monet, D., Noecker, C., Peale, S., Quirrenbach, A., Seager, S., and Winn, J., "Worlds beyond: A strategy for the detection and characterization of exoplanets," **Worlds Beyond: A Strategy for the Detection and Characterization of Exoplanets** (2008). [arXiv:0808.2754].

[30] Coudé du Foresto, V., Absil, O., Beaulieu, J.-P., Beichman, C., Boccaletti, A., Chakraborty, A., and et al., "Blue dots report," **Blue Dots report** (2010). http://www.blue-dots.net.

[31] Hatzes, A., Boccaletti, A., Dvorak, R., Micela, G., Morbidelli, A., Quirrenbach, A., Rauer, H., Selsis, F., Tinetti, G., and Udry, S., "A european roadmap for exoplanets," **Exoplanet Research Advisory Team Report** (2010). http://sci.esa.int/eprat.

[32] Smith, D. R., Walton, D. M., Ingley, R., Holland, A. D., Cropper, M., and Pool, P., "Emccds for space applications," in [*SPIE Conf. Series*], *SPIE Conf. Series* **6276**, 62760K (2006).

[33] Grasset, O., Schneider, J., and Sotin, C., "A study of the accuracy of mass-radius relationships for silicate-rich and ice-rich planets up to 100 earth masses," *ApJ* **693**, 722–733 (2009).

[34] Fortney, J. J., Marley, M. S., and Barnes, J. W., "Planetary radii across five orders of magnitude in mass and stellar insolation: Application to transits," *ApJ* **659**, 1661–1672 (2007).